New inventory of dust emission sources in Central Asia and Northwestern China derived from MODIS imagery using dust enhancement technique

JGR Atmospheres

RESEARCH ARTICLE
10.1029/2020JD033382

New Inventory of Dust Emission Sources in Central Asia and Northwestern China Derived From MODIS Imagery Using Dust Enhancement Technique

Mohamad Nobakht[1,2], **Maria Shahgedanova**[1], **and Kevin White**[1]

[1]Department of Geography and Environmental Science, University of Reading, Reading, UK, [2]Telespasio VEGA UK Ltd., Luton, UK

Key Points:

- New data set on dust emission point sources has been derived from MODIS imagery for Central Asia and northwestern China
- Eastern and northern Taklimakan, Aralkum, Amu Darya, Syr Darya, and Uzboy valleys are the most persistent sources of dust
- Dust sources were associated with wildfire scars in the north and changing lake levels, irrigation and agricultural practices in the south

Supporting Information:

- Supporting Information S1

Correspondence to:
M. Shahgedanova,
m.shahgedanova@reading.ac.uk

Citation:
Nobakht, M., Shahgedanova, M., & White, K. (2021). New inventory of dust emission sources in Central Asia and northwestern China derived from MODIS imagery using dust enhancement technique. *Journal of Geophysical Research: Atmospheres*, *126*, e2020JD033382. https://doi.org/10.1029/2020JD033382

Received 3 JUL 2020
Accepted 28 JAN 2021

Author Contributions:
Conceptualization: Mohamad Nobakht, Maria Shahgedanova, Kevin White
Formal analysis: Mohamad Nobakht
Investigation: Mohamad Nobakht
Methodology: Mohamad Nobakht, Maria Shahgedanova, Kevin White
Supervision: Maria Shahgedanova, Kevin White
Validation: Mohamad Nobakht
Writing – original draft: Maria Shahgedanova
Writing – review & editing: Mohamad Nobakht, Kevin White

Abstract The first inventory of dust emission sources in Central Asia and northwestern China (35–50°N, 50–100°E) derived from the twice daily MODIS imagery from 2003 to 2012 is presented. A high-resolution (1 km) dust enhancement product was generated to produce maps of dust point sources (DPS), indicating geographical locations of the observed dust emissions, and gridded data sets of dust emission frequencies. About 13,500 DPS were detected over an area of $\sim 5 \times 10^6$ km^2, however, their distribution was uneven. The highest frequency of DPS occurred in the northern and eastern Taklimakan, in the Aralkum, and in the regions, which were not widely reported in literature before, the Balkh delta in northern Afghanistan and the pre-Aral, from the northern Caspian coast to the Betpak-Dala desert in Kazakhstan. South of the Aral, DPS were mainly associated with fluvial features: drying lakes, dry river beds, alluvial deposits and agricultural activity which is closely linked to water availability in this arid region. In the pre-Aral and Balkhash-Junggar regions, land damaged by wildfire was the main source of dust. In China and eastern Kazakhstan dust emissions peaked in spring; in Central Asia and western Kazakhstan—in summer. The Aralkum was active throughout the year with a positive trend in emission frequency over the study period. Locations of DPS did not always correlate with high atmospheric optical depth (AOD) particularly west of the Aral and in the southern Taklimakan where few DPS were detected despite the high AOD values. This was attributed to dust transport from the upwind sources.

Plain Language Summary Desert dust plays an important role in the global environmental system and affects climate, crops, human health, and even enhances glacier melt. It is important to know where and when dust storms occur in order to model the dust cycle and help manage land. We analyzed satellite imagery to identify the observed dust storms in Central Asia and northwestern China and created the first regional database of dust sources, including their location, time of dust storm formation, associated landforms and weather conditions. The study region accommodates some of the world's largest deserts and a new desert, the Aralkum, which developed in the former Aral Sea. The largest number of dust sources were found in the northern and eastern Taklimakan followed by the Aralkum, where the frequency of dust storms increased over time. Many dust sources were found in northern Afghanistan and western Kazakhstan, which were not widely reported before. South of the Aral Sea and in the Taklimakan, dust emissions were mainly associated with fluvial features: drying lakes, dry river beds, alluvial deposits, and agricultural activity, which is closely linked to water availability in this arid region. North of the Aral, land damaged by wildfire was the main source of dust.

1. Introduction

Mineral dust plays an important role in climate system, affecting energy balance on local, regional and global scales (Goudie, 2009; Mahowald et al., 2010; Painter et al., 2012; Shao et al., 2011; Washington et al., 2003). It affects nutrient cycles in the terrestrial and marine biosphere (Shao et al., 2011) and contributes to the deterioration of air quality and human health (Sternberg & Edwards, 2017). Globally, about 30% of the total land area is a potential source of mineral dust for the atmosphere. There is uncertainty about how this area and dust emissions will change in the future in response to human activities and climate change. Several studies (Ginoux et al., 2012; Mahowald, 2007; Prospero et al., 2002) suggest that dust emissions will grow potentially leading to stronger impacts both locally and in distant regions while other highlight

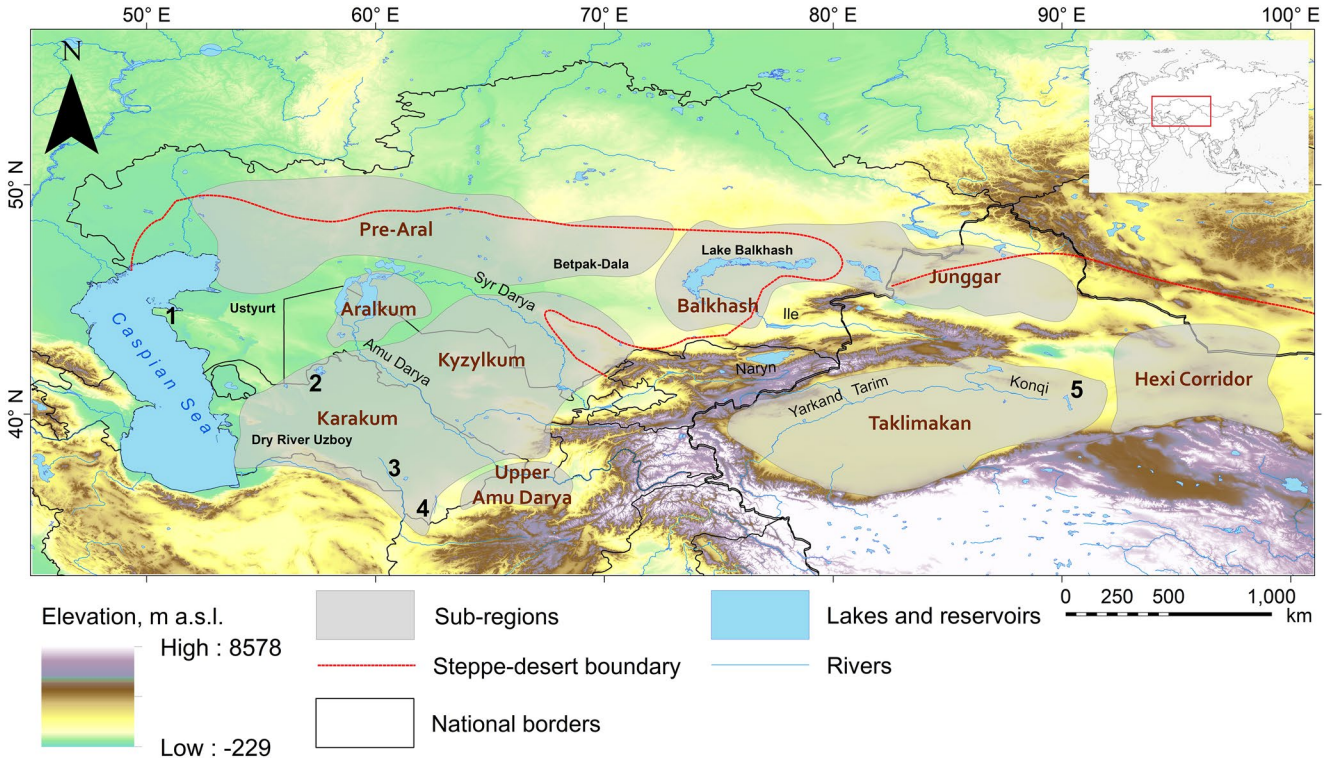

Figure 1. Main dust source regions in Central Asia. These regions were used in the calculation of the dust source statistics. Numbers on the map denote geographical locations mentioned in the text: 1—Mangyshlak peninsula; 2—Lake Sarygamysh; 3—River Tejen; 4—River Murghab; 5—Lake Lop Nur.

complex and spatially nonhomogeneous response of dust emissions to climate change and variability (Chin et al., 2014; Xi & Sokolik, 2015a).

There is extensive research on source regions, entrainment processes, and transportation of mineral dust in the atmosphere (Shao et al., 2011). The latter is most frequently characterized by Atmospheric Optical Depth (AOD) measured either *in situ* by the Aerosol Robotic Network (AERONET; Holben et al., 2001) or using remote sensing (e.g., Ginoux et al., 2010; 2012). Other records of dust-related indices are available with a long-term global coverage, for example, the Total Ozone Mapping Spectrometer (TOMS) product (Washington et al., 2003). The Spinning Enhanced Visible and Infrared Imager (SEVERI) was used to develop regional inventories of dust emissions with very high temporal resolution in the regions covered by the Meteosat Second Generation (MSG) geostationary satellite, that is North Africa (Schepanski et al., 2009) and the Middle East (Hennen et al., 2019). There is a growing number of publications on mineral dust entrained from the deserts of China and Mongolia (e.g., Che et al., 2013; Shao & Dong, 2006; Qian et al., 2007; Wang et al., 2008, 2006; Xuan & Sokolik, 2002).

Information on mineral dust in Central Asia (CA) and northwestern China (NWC), which accommodate vast deserts and dry steppes (Figure 1), including spatial distribution of sources, temporal trends in their activity, and atmospheric pathways of dust is more limited, although the importance of this region in the global dust cycle, and the role of changes in land cover leading to alterations in dust emissions, are recognized (Groisman et al., 2017; Indoitu et al., 2012; 2015; Monier et al., 2017; Sternberg, 2017; Wang et al., 2008). Regional economic activity, including agricultural production, and the health of millions of people are affected by dust storms and high concentrations of mineral aerosol (Orlovsky et al., 2005; Sternberg, 2017). Deposition of desert dust on the snow pack and glaciers in the Tien Shan, Pamir, and Hindukush significantly alters surface albedo, creating positive at-surface radiative forcing and enhancing snow and ice melt (Painter et al., 2012).

Research on dust storms began in the 1930s in CA and in the 1960s in NWC when regular monitoring of dust storms was introduced at regional meteorological stations. Analyses of changes in dust storm

frequency, based on these data and covering the period between the 1960s and 2000s, were published by Indoitu et al. (2009) and Issanova et al. (2014; 2015a; 2015b) for CA and by Wang et al. (2006) for NWC. In the 1980s, when the desertification in the Aral Sea region was first reported, data acquisition campaigns were conducted, collecting a wide range of data on optical and radiative properties of desert dust (Hansen et al., 1993; Sokolik & Golitsyn, 1993) and meteorological conditions of dust storm formation (Smirnov et al., 1993). Following the breakdown of the USSR, data were mostly obtained through field campaigns in the Aral Sea region (e.g., Groll et al., 2013). There is a growing number of field studies in NWC (Wang et al., 2008). Currently, there are four operational AERONET sun photometers in Kyrgyzstan, Tajikistan, and the Muztag-Ata mountains in China. Ground-based lidar measurements (Hofer et al., 2017; 2020) and regular $PM_{2.5}$ and PM_{10} sampling (pers.com., Dr. S. Abdulaev, Physical Technical Institute of the Academy of Sciences of Tajikistan) are conducted in Tajikistan. China Aerosol Remote Sensing Network (CARSNET) began operating in NWC in 2002 (Che et al., 2015).

The use of remote sensing, particularly the Deep Blue AOD retrieval algorithm (Hsu et al., 2004), introduced in Collection 5.1 (C5) of MODIS aerosol products, enabled improved retrieval of aerosol properties over deserts, resulting in the expansion of dust AOD data collection globally. Ginoux et al. (2012) used this approach to characterize global distribution of desert dust in the atmosphere during the 2003–2009 period. However, the focus was on eastern Asia and the Middle East, while CA was represented to a limited extent. Further research showed that the Deep Blue AOD of mineral dust was underestimated in comparison with the AERONET measurements, especially over deserts (Shi et al., 2013) and, although this comparison was performed specifically for North Africa, the same limitation is likely to apply in CA (Xi & Sokolik, 2015a). The Enhanced Deep Blue (E-Deep Blue) aerosol product was introduced in Collection 6 (C6) of MODIS products as an improved version of the C5 Deep Blue product, enabling the extension of spatial coverage from the bright reflecting regions to the entire cloud-free and snow-free land area and reducing uncertainty of retrievals (Sayer et al., 2013). The C6 AOD was used by Xi and Sokolik (2015a) in combination with simulated dust emissions to analyze interannual variability and trends in dust load over CA, identifying a negative trend in dust activity attributed to decreasing surface wind speeds.

Several studies (Ginoux et al., 2012; Xi & Sokolik, 2015a; 2015b) used AOD to characterize dustiness over CA and NWC highlighting the diversity of land-cover and land-use types contributing to dust emissions and varying sensitivity of dust fluxes to meteorological conditions. However, these and other studies using AOD were based on the retrievals of aged dust in the atmosphere, potentially displaced from its sources. There is a lack of detailed identification of actual dust sources, land-surface properties resulting in dust emissions, temporal trends and characterization of conditions of dust source activation (DSA) in CA in contrast to other major dust source regions for which this information is more widely available, for example, the Sahara (Schepanski et al., 2007; 2009) and the Middle East (Hennen et al., 2019). Wang et al. (2006; 2008) discussed dust storm climatology in the Taklimakan in the context of land surface characteristics. A detailed analysis, characterizing erodible land surfaces and statistics of individual dust plume formation was produced by Walker et al. (2009) using MODIS imagery for the southwestern part of the region including Afghanistan, Iran and Pakistan. For the rest of CA, such information is not available limiting our understanding of the dust cycle in CA, our ability to model dust transport, to forecast dust storms, and manage land.

This paper presents the first large-scale inventory of observed dust emissions and dust point sources (DPS) from which these emissions originated in CA and NWC, derived from twice daily MODIS imagery over the 2003–2012 period. We use the term DPS instead of "dust storm" because the latter can originate from multiple sources. DPS characterization of dustiness is different from that provided by AOD and discussed by Ginoux et al. (2012) and Xi and Sokolik (2015a; 2015b) because DPS show actual emission sources while AOD shows the spread of the aged dust in the atmosphere. The two types of data are complimentary and in the future, DPS can be used as a control data set to resolve differences between the observed AOD and modeled dust entrainment (e.g., Xi & Sokolik, 2015a).

The objectives of this paper are to: (i) present DPS statistics including its locations and temporal variability; (ii) compare DPS locations with spatial distribution of AOD and Dust Optical Depth (DOD); (iii) briefly discuss landforms, land cover and land use types contributing to the formation of DPS. Meteorological conditions leading to the formation of dust storms and transportation of dust are addressed briefly and their detailed discussion will be presented elsewhere.

2. Data and Methods

The main data set produced by this study comprises DPS, which are defined as geographical locations of every single dust outbreak detected between January 2003 and December 2012. In addition, AOD values were derived as a supplementary data set to compare DPS locations with dust present in the atmosphere. MODIS Terra and Aqua acquisitions from overpasses between 10:30 and 13:30 local time (depending on location in the region), respectively, were used to generate both data sets. MODIS data were retrieved from NASA Level 1 and Atmosphere Archive and Distribution System (LAADS; https://ladsweb.nascom.nasa.gov) (Table S1).

2.1. Dust Optical Depth

Daily C6 MODIS Level-2 swath products MOD04 (Terra) and MYD04 (Aqua) datasets respectively were obtained as Hierarchical Data Format—Earth Observing System (HDF-EOS) granules for 2003–2012. Each granule covers 5 min of observation time along the satellite track or an area of 2,030 km along the path by 2,330 km along the swath (Savtchenko et al., 2004). Over 43,000 granules were obtained from the LAADS repository to produce daily raster mosaics for the study region at the ground resolution of $0.1° \times 0.1°$. The AOD retrievals by the Aqua satellite (MYD04) were used. Importantly, no AOD retrievals were available in MODIS C6 for the Aralkum due to the use of static surface reflectance model in AOD retrieval algorithm (pers. com., Dr. A. Sayer, MODIS AOD Developing Team, NASA Goddard Space Flight Center) and DOD was not calculated for this region.

To detect the location of dust hotspots (Gillette, 1999), frequency of occurrence of DOD (FO-DOD) and its spatial distribution were derived. The DOD datasets were constructed by applying three screening criteria to the AOD retrievals (Table S1): (i) Ångström Exponent (AE) less than 0.5; (ii) SSA at 412 nm less than 0.95; and (iii) increase of single scattering albedo with wavelength. Criterion (i), restricting the AOD observations to larger particles, is based on the inverse relationship between AE and dust particle size. Deposition of large dust particles is controlled by gravitational settling. They are likely to occur close to sources of dust emissions and indicate the presence of dust sources (Knippertz, 2014). However, this criterion can be satisfied in the absence of desert dust in coastal regions (e.g., the Caspian or Aral) or in proximity to other saline lakes (widespread in CA) where concentrations of coarse salt particles are high. To filter out salt particles, criterion (ii) was applied based on the higher SSA of sea salt (close to 1) in comparison with mineral dust. Criterion (iii) is based on a specific property of mineral dust - a positive difference between SSA at 650 nm and SSA at 412 nm (Ginoux et al., 2012). This three-step screening procedure was evaluated successfully by Ginoux et al. (2012) using AOD data from AERONET.

A ratio between number of days with DOD exceeding 0.2 (a threshold for background AOD; Ginoux et al., 2010) to the total number of AOD retrievals for the same season was calculated for each season and each grid cell and expressed as frequency of occurrence (%) of DOD values (FO-DOD). To avoid miscalculation over regions with scarce AOD retrievals, which can result from the complex background reflectivity, FO calculations for grid cells with less than 10% of AOD retrievals during the whole time period were discarded. The FO-DOD data were summarized as seasonal maps (Figure S1).

2.2. Development of DPS Data Set: Dust Enhancement

Detecting dust over the land surface, and particularly over deserts, using visible-shortwave infrared (solar spectrum) optical satellite imagery is challenging because mineral aerosol and the background desert surface have similar reflectivity in this part of the spectrum (Baddock et al., 2009). This problem can be resolved by using dust enhancement techniques based on a brightness temperature difference (BTD) between the warmer ground surface and cooler elevated dust plumes, derived using emitted infrared (IR) and thermal infrared (TIR) bands (Baddock et al., 2009; Miller, 2003). This approach, however, can lead to potential misclassification of dust in the presence of cirrus clouds, which are cooler than the surface, and can be falsely identified as dust when IR/TIR channels only are used. To avoid this problem, we used the dust enhancement method (Miller, 2003) which combines a conventional BTD technique with information from reflective solar radiation bands (Table S1) to improve visual detection of dust events (Figure 2).

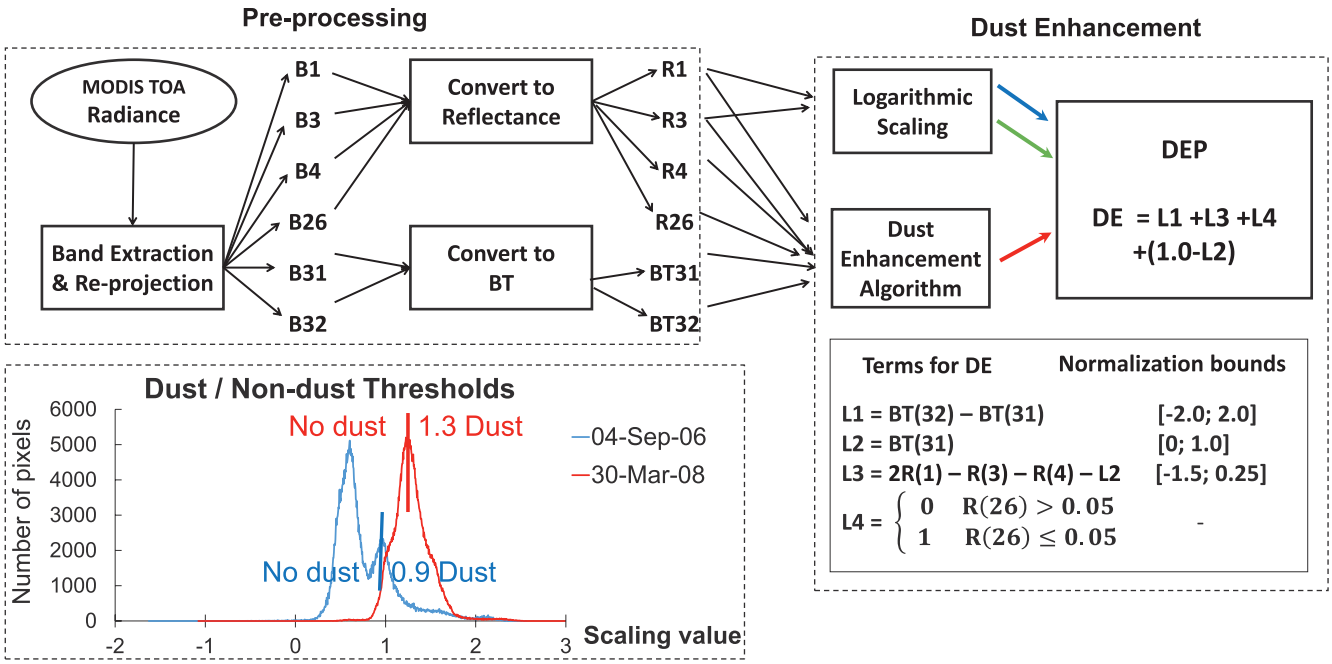

Figure 2. Schematic procedure for generating daily Dust Enhancement Product (DEP) images from MODIS data and examples of histograms for two dust events in the Balkhash region illustrating method for determining dust/nondust thresholds. Thresholds are marked by vertical bars and scaling values are shown. MODIS band (B) information is given in Table S1. BT is brightness temperature; R is reflectance; and DE is dust enhancement values over land. Terms for DE are from Miller (2003). Dust event observed on 30 March 2008 is shown in Figure S3.

The dust enhancement algorithm is based on the following principles: (i) elevated dust produces lower brightness temperature against the hot land surface background; (ii) dust can be discerned from clouds having the same radiometric temperature based on its spectral properties; (iii) dust often produces a positive reverse BTD between MODIS bands 32–31 (12–11 μm); and (iv) information from the additional infrared MODIS Band 26 (1.38 μm) enables distinguishing between dust and cirrus clouds. Normalization bounds were determined by Miller (2003) experimentally from a wide variety of dust case studies over land and values were selected to optimize dust contrast while maintaining an enhancement appearance consistent with the over-water algorithm. The algorithm (Figure 2) generates Dust Enhancement Product (DEP) based on the exceedance of a dimensionless statistics (DE). DEP is presented as Red-Green-Blue (RGB) composite. Blue and green color guns are loaded with MODIS Bands 3 and 4 reflectance. For better visualization, the reflectance values falling within [−1.45, 0.0] are byte-scaled between [0, 255]. The red color gun is loaded with DE values. In RGB image, dust is visually differentiated as shades of pink, while clouds and land appear as cyan and green, respectively.

The definition of DE thresholds, discriminating between dust and nondust, involved compilation and examination of pixel histograms (Figure 2). In each histogram, peaks were found and attributed to the specific scene components such as clouds or aerosol and threshold values, which represent the presence of dust in the scene best, were determined by the operator. The thresholds are sensitive to varying atmospheric conditions, surface reflectance, dust concentrations and mineralogy and need to be calculated for relatively small regions where dust sources have similar properties or even specifically for each dust event (Baddock et al., 2009; Darmenov & Sokolik, 2005). The use of the scene- or event-specific thresholds was shown to improve the recognition of dust significantly (Baddock et al., 2009). In this study, thresholds were derived for individual scenes (e.g., 0.9 for September 4, 2006 and 1.3 for March 30, 2008; Figure 2). If preliminary inspection indicated that multiple sources of dust were present, pixel histograms were resampled for dust-emitting areas within the scene to adjust dust/nondust threshold and enhance dust visualization. Therefore, DE thresholds varied temporally and between regions.

Examples of DEP images are shown in Figures S2 and S3. Dust plumes, highlighted as pink can be clearly distinguished from other features in the scene and were used to determine locations of DPS.

2.3. Identification of DPS and Compilation of the Data Set

Daily DEP images were generated from MODIS Terra and Aqua L1B Top of the Atmosphere (TOA) radiance data for the period between January 1, 2003 and December 31, 2012 for the study region (Figure 1). For both Terra and Aqua satellites, on average, seven granules were required to generate a daily mosaic covering the study area between 35–50°N and 50–100°E. Six spectral bands were extracted from each MODIS granule (Table S1; Figure 2). The data were re-projected from the MODIS native swath projection to WGS84 system at a 0.01° (~1 km) resolution using the associated MODIS geolocation products (MOD03) and MODIS Re-projection Tool (MRT; https://lpdaac.usgs.gov/tools/modis_reprojection_tool) and used to create two daily mosaics of 5,000 × 1,500 km encompassing the study region at 0.01° (~1 km) resolution.

The ~2-hour time difference between the two overpasses enabled the investigation of the development of individual dust plumes between the two snapshots and establishing locations of DPS at the head of each dust plume with greater precision. While the DE method distinguishes between clouds and dust more efficiently than other methods, it is known to be sensitive to changes in ground surface reflectance. Baddock et al. (2009) demonstrated potential misclassification of ephemeral lakes and fire scars (areas de-vegetated by wildfire; Figure S4), which are potential sources of dust, as emitting dust sources. Walker et al. (2009) showed that false enhancement is possible over the cold terrain, particularly in winter and in the mornings. Inspection of two consecutive MODIS scenes for dust plume dispersion as well as additional imagery such as DOD and visible MODIS (e.g., Figure S2) helped to reduce this uncertainty.

DPS were identified manually and archived using the following procedure:

(i) The DOD and DEP images were visually inspected. Although DOD, which has 10 km spatial resolution, does not necessarily capture point locations of DPS, it confirmed the occurrence of dust events pointing at the need for pixel histogram resampling and potential adjustment of thresholds for different events within a scene, and reduced risk of dust misclassification

(ii) Dust emitting areas were visually determined and DPS marked as DSA events on the twice-daily DEP images. Manual mapping was successfully used before to map dust sources in the Sahara (Schepanski et al., 2007) and the Middle East (Hennen et al., 2019). To avoid bias created by increasing observer skill over time, the operator (M. Nobakht) trained on a year of data prior to the compilation of the DPS data set. Two control steps were introduced. (1) The upwind location of the dust plume had to be unchanged in both Terra and Aqua images. In majority of the events, the operator could visually observe the dust plume expansion between the two overpasses, while the head of the plume (recorded DPS) was at the same location in both snapshots. (2) If DPS were visible on a single overpass image, auxiliary information about dust emitting surfaces (v) was used to confirm DPS location

(iii) Locations (latitude, longitude) of all activated DPS and date of emission were recorded. If DPS appeared on both Terra and Aqua images on the same day, they were only recorded once. If emissions from DPS continued for several consecutive days, these DPS were recorded for each day. There was no discrimination between the intensity of dust storms

(iv) In order to characterize uncertainty in the DPS data, "Quality Flags" (QF) on a scale of 1–3 were assigned to every recorded DPS. Criteria for QF assignment are shown in Table S2. QF1 corresponded to the most reliable data whereby DPS was clearly visible and there were no clouds or overpassing dust plumes (e.g., Figure S2b) and QF3 corresponded to the DPS partially obscured by meteorological or dust clouds (Figure S3)

(v) Auxiliary data were examined to increase confidence in locating DPS and gather information about the nature of the eroding surfaces including GTOPO30 global DEM at 1 km spatial resolution (available from the U.S. Geological Survey) and high-resolution satellite optical imagery for dust-free days (e.g., Worldview, GeoEye, Landsat, SPOT, and Ikonos) obtained from various sources

(vi) The ERA Interim reanalysis surface wind data were recorded for the time and location of dust events and later updated to ERA5

Locations of all identified DPS, timing of dust events, auxiliary data and meteorological variables formed an inventory of DPS in CA and NWC. DPS locations were plotted against FO-DOD to compare the data sets. In addition, number of days with DSA were calculated and binned in 1° × 1° grid. Days with at least one DPS activation in a grid cell were considered as DSA days. The DSA maps do not account for the number of DPS in the grid cells and characterize frequency but not intensity of dust events.

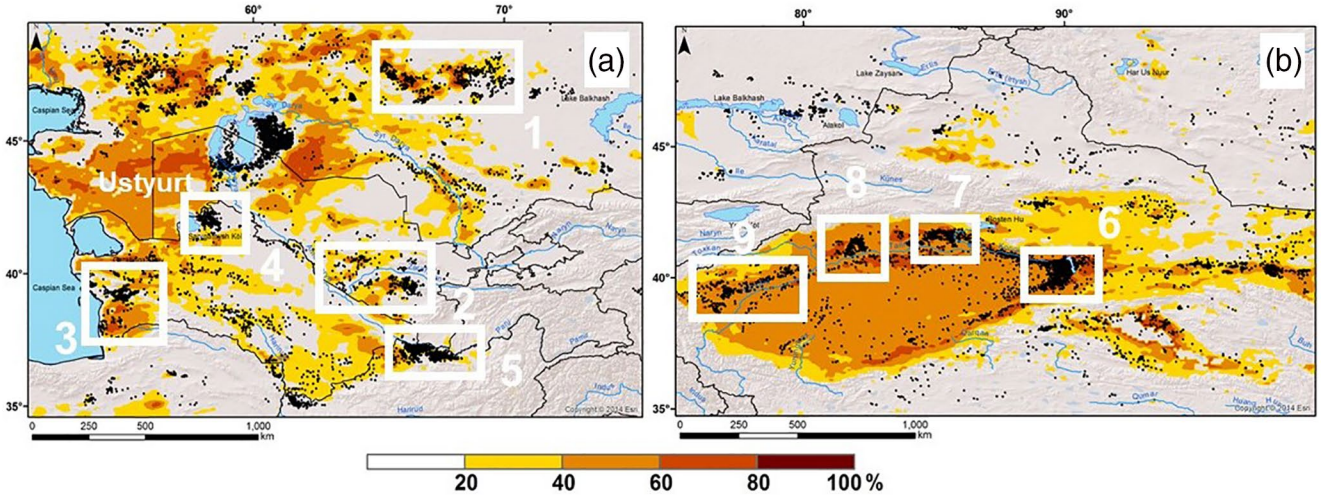

Figure 3. Locations of DPS (black dots) in (a) CA and (b) NWC and eastern Kazakhstan. The summer and spring FO-DOD (Figure S2) are used as background in (a and b), respectively. Regions, mentioned in the text, are highlighted. (a): 1—Betpak-Dala; 2—lower reaches of the Zeravshan and Samarkand region; 3—dry River Uzboy and River Atrek deltas; 4—Sarygamysh depression; 5—the Balkh delta (upper Amu Darya). (b): 6—Lake Lop Nur; 7—the Konqi alluvial fan; 8—the Aksu and Muzart; 9—the Yarkand. See Figures S5 and S6 for the high-resolution satellite images of geomorphological setting of the highlighted regions. CA, Central Asia; DPS, dust point sources; NWC, northwestern China.

3. Results

3.1. Spatial Distribution of DOD

Seasonal FO-DOD values greater than 0.2 (Figures 3 and S1) confirmed that dust activity peaks in spring in the eastern and in summer in the western part of the region (Aoki et al., 2005; Che et al. 2013; Ginoux et al., 2012; Xi & Sokolik, 2015a) although several hotspots remain active throughout the year. In CA, FO-DOD peaked in summer and in spring in the following regions (Figures 3a and S1): (i) in the pre-Aral region-west and north of the Aral Sea over the Mangyshlak peninsula, Ustyurt plateau, and the Betpak-Dala desert where it reached 80% in these seasons; (ii) in the middle reaches of the Syr Darya and Amu Darya over the Kyzylkum desert (where FO exceeds 20% even in autumn and winter); (iii) in the central and southern Karakum desert particularly over the dry River Uzboy valley (where FO values exceed 40% throughout the year); and (iv) in the River Balkh delta (upper Amu Darya) in northern Afghanistan. In the Taklimakan, FO-DOD peaked in spring when the FO values ranged between 60% and 80% across the region. Seasonal values of AOD ranged between 0.45 (a very low value observed in 2005) and 1.0 in 2006–2007. This is considerably higher than elsewhere in the study area. In summer, the FO-DOD values declined sharply across the region to 20%–40% with the exception of the northern and eastern margins of the Taklimakan and the Tarim valley (Figures 3b and S1) and seasonal AOD values were lower at 0.4–0.6.

3.2. Dust Point Sources

Overall, 13,500 DPS were registered in the study area in the 2003–2012 period. Spatial distribution of the identified DPS is summarized for two sub-regions: (i) CA (north and south of the Aral Sea) and (ii) NWC and eastern Kazakhstan (Figure 3) comparing DPS locations with the summer and spring FO-DOD values, respectively.

3.2.1. Central Asia: North of the Aral Sea

A large number of DPS were registered in the dry steppes and semi-deserts of Kazakhstan extending from ~55°E to in the pre-Aral to 70°E in the Lake Balkhash region (Figure 3). Locations of DPS clusters did not always coincide with maxima in DOD. For example, the pre-Aral and Betpak-Dala, where clusters of DPS were identified, featured high FO-DOD values while the Balkhash region did not (Figure 3a).

Degradation or removal of vegetation cover, predominantly by wildfire but also by overgrazing, were identified as the main processes leading to the formation of dust storms in the pre-Aral and Betpak-Dala. Fire scars remaining on the burned land were detectable on satellite imagery and dust emissions were traced back to the fire scars, identifying them as activated DPS (Figures S2 and S3). The amount of time required for the vegetation and biological soil crust to be restored over the burned areas is determined by a combination of burn severity, soil type and climatic conditions (Strong et al., 2010). In CA, fire scars remained active sources of dust for several years except in a few areas which regained their vegetation cover shortly after the onset of the wet season.

3.2.2. Central Asia: South of the Aral Sea

In this region, DPS were associated predominantly with fluvial features but also with agricultural landscapes which, for millennia, were developing in the proximity to water leading to the degradation of several water bodies, most notably the Aral Sea, in the 20th Century.

The highest density of DPS identified in this study characterized a newly developed desert, the Aralkum (Figure 3a). Approximately 59% of the DPS registered in the Aralkum occurred in the northern and eastern sectors of the desiccated lake where loamy deposits are the prevailing soil type and dry solonchaks are widespread (Kozhoridze et al., 2012). Around 20% of the observed DPS occurred in the southern and southeastern parts of the lake where lighter sandy and sandy-loamy soils prevail. The remaining 21% were registered on the exposed lake bed between the former Amu Darya delta and Vozrozhdeniya Island which was a site for biological and chemical weapons testing in the 1950–1990s. Decontamination was carried out in 2002 but there is potential risk of contamination of dust emitted from this region by remaining toxic pathogens (Micklin, 2007). Importantly, very few DPS were detected on the Myngyshlak peninsula and virtually none on the Ustyurt plateau, west of the Aralkum, which were characterized by the highest AOD and FO-DOD values in this (Figures 3a and S1) and in previous studies (Xi & Sokolik, 2015a).

Further south, FO-DOD values peaked over the Kyzylkum desert between the Syr Darya and the Amu Darya Rivers (Figures 3 and S1). Here, DPS were recorded in relatively narrow zones on the floodplains in the middle courses of both rivers. Over 160 DPS were recorded along the nearly 400 km stretch of the Syr Darya and its tributary, the Arys, in southern Kazakhstan where a decline in the extent of irrigated land in the 1990s resulted in erosion of the abandoned fields (Baitulin, 2001). Similarly, agricultural lands in the lower reaches of the Zeravshan River and in the Samarkand region in Uzbekistan were also vulnerable to wind erosion, leading to the formation of an active cluster of DPS (Figures 3a and S5).

In the Karakum, DPS were associated with fluvial features, both modern and ancient (Figure 3). A large number of DPS occurred along the 750 km long dry channel of the ancient River Uzboy (Figure S5a) which in the past connected Lake Sarygamysh with the Caspian Sea, but has been dry for at least 800 years (Velichko & Spasskaya, 2002). A cluster of multiple DPS, accounting for about 17% of all DPS in the Karakum-Kyzylkum region, was registered in the Uzboy and Atrek delta (Figure 3a). A high concentration of DPS occurred in the Sarygamysh depression (Figures 3a and S5b) particularly east of Lake Sarygamysh on a flat lowland composed by the alluvial deposits left by the migrating Amu Darya channel (Orlovsky et al., 2012). It accounted for ~15% of all DPS registered in the Karakum-Kyzylkum. The lake dried in the 18th Century following the natural migration of the Amu Darya course toward the Aral Sea (Létolle et al., 2007) but was restored in the 1960s to collect irrigation wastewater. The influx of water varies interannually and seasonally, causing strong fluctuations in the lake's level exposing both old and modern alluvial sediments (Kostianoy et al., 2013; Orlovsky et al., 2012).

DPS clusters were frequently associated with alluvial fans forming in river deltas. Two particularly active clusters, associated with these landforms, were identified in the Balkh delta in northern Afghanistan and in the deltas of the Tejen and Murghab Rivers in southern Turkmenistan (Figures 3a and S5e). The former region was characterized by the second highest identified DPS density, after the Aralkum and, together with the Aralkum and Sarygamysh regions, can be viewed as area (rather than points) source of dust.

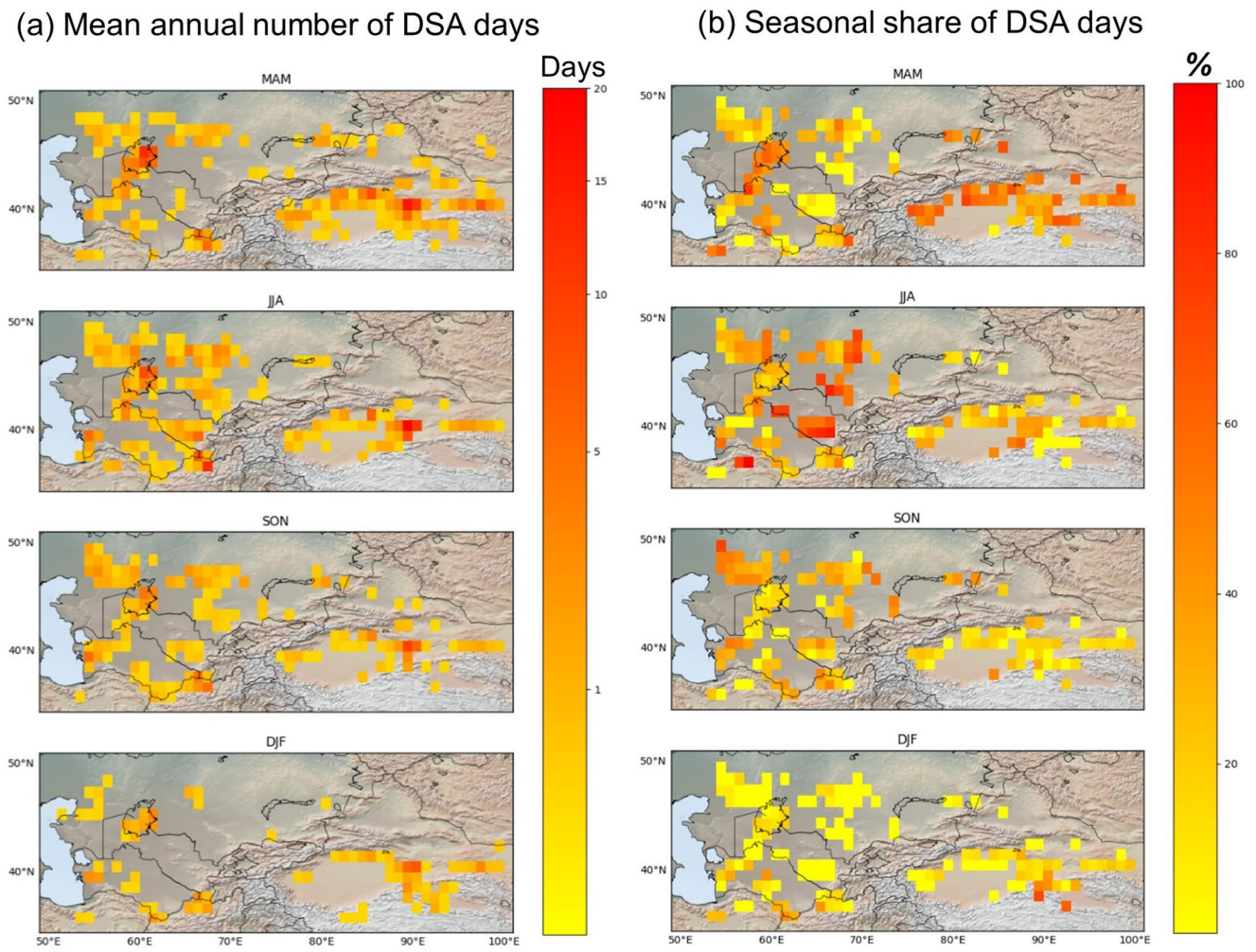

Figure 4. Mean seasonal statistics of DSA averaged over the 2003–2012 period. Grid cells with less than one dusty day per year are transparent. DSA, dust source activation.

3.2.3. Northwestern China

The Taklimakan desert in NWC produced the largest number of DPS in the region, accounting for 35% of all dust events registered across the entire study area (Figure 3b). These were located predominantly along the Tarim River and around Lake Lop Nur in the east. Prior to the construction of reservoirs and irrigation systems in the mid-20th Century, the Tarim emptied into Lake Lop Nur. Now the Lop Nur is a salt-encrusted lake bed (Middleton, 1986) producing a major cluster of DPS (Figures 3b and S6a). The eastern margin of the Taklimakan, including the Lop Nur, was the most active and persistent area source of dust where over 2,200 DPS (a half of all DPS in this region) were recorded (Figure 3b) and activated most frequently (Figure 4).

The Tarim's runoff is formed by snow and glacier melt in the Tien Shan and Kunlun and 60%–80% of the runoff occurs between June and August, carrying over 80% of the annual sediment load (Rittner et al., 2016; Ye et al., 2014). In the remaining months, high air temperature and falling river stage allow the alluvial fans and flood plains to dry out, becoming active sources of dust. The alluvial fans of the River Konqi and Rivers Aksu and Muzart account for 13% and 9% of the Taklimakan DPS, respectively (Figures 3b, S6b, and S6c). These fans support agricultural production, and dust events occur primarily at the margins of the agricultural land and at the abandoned or degraded farmland. Similarly, a cluster of DPS on the Yarkand River, west of the Aksu (Figure 4b), formed as a result of poor farming practices and overgrazing (Rittner

et al., 2016). Although the southern Taklimakan was characterized the by very high FO-DOD values in spring and summer (Figure S1), there were few DPS in its central and southern sectors (Figure 3b). This discrepancy is addressed in Section 4.2.

A large number of DPS were recorded in the Hexi corridor and in the Qaidam Basin where FO-DOD values were also high. By contrast, in the Junggar region, merging into the Balkhash depression in the west, a relatively large number of DPS was detected overall but because of their low density and infrequent activation, FO-DOD values were low (Figures 3b and S1). Thus in the Hexi Corridor, DPS were activated 26–45 times per year and in the Balkhash-Junggar region, 10–18 times increasing to 32–34 in 2004–2006 (Figures 5 and 6). In contrast to other sub-regions, Balkhash-Junggar is predominantly dry steppe characterized by higher threshold friction velocity than any other sub-region (Xi & Sokolik, 2015b).

3.3. Spatial Patterns and Interannual Variability in DPS Activation

Figure 4 presents frequency of DSA days averaged over the 2003–2012 period. Neither DPS nor DSA days statistics provides information about the intensity of dust storms. To obtain a proxy measure of intensity of dust events, the average number of DPS per DSA day was calculated for each year (Figure 5).

The eastern part of the Tarim basin exhibits the highest frequency of DSA days. In the Lop Nur region and lower reaches of the Konqi River, on average over 50 and 25 days with dust events per year, respectively, were observed (Figure 4). The frequency of DSA in the Taklimakan was highest in 2006 and lowest in 2011 reaching 113 and 76 days, respectively (Figure 5a). Both in this region and in the Hexi Corridor (Figure 5b), there were no consistent temporal trends either in DSA frequency or in number of DPS activated per day.

The second most active region was the Aralkum with over 30 DSA days per year (Figure 4). During the study period, the mean number of DSA days increased from 32–18 in 2003–2004 to 62 in 2012 (Figure 5e) due to the desiccation of the eastern Aral following its detachment from the Small Aral in 2005. The number of DSA increased in all seasons except winter but the strongest trend was observed in spring (Figure 5h). The number of DPS per day increased after 2006 too, indicating more intense dust storms. This is in line with the reported doubling of dust storms over the Aral (Indoitu et al., 2012) and increase in the frequency of high-intensity dust deposition events (Groll et al., 2013) registered by the regional meteorological stations. The frequency of DSA days and average number of DPS per day increased in the Karakum-Kyzylkum region from about 30 and 2–3 in 2003–2005 to 40–80 and 3–4 in 2006–2012, respectively (Figure 5f) in all seasons including winter indicating that, in addition to changes in the lake level, climatic variability might have affected dust storm activity. Statistically significant negative trends in annual precipitation in the 1982–2012 period were reported for the Aralkum and Karakum region by Jiang et al. (2019). By contrast, number of DPS and DSA days declined in the Balkhash-Junggar region in all seasons except winter (Figures 5c and 5i). A weak positive trend in annual precipitation and, probably, pasture abandonment and decline in livestock reverting overgrazing may explain these trends (Jiang et al., 2019).

3.4. Seasonal Cycles of DPS Activation

Seasonal statistics of DSA days are summarized in Figures 4 and 6. Similarly to FO-DOD (Figure S1), a spring maximum characterizes NWC and the Balkhash-Junggar region. Dust storms are observed in the northern Taklimakan and Hexi Corridor almost throughout the year from February to October, starting and peaking earlier in the east (in February and March–April, respectively) and about a month later in the west. A secondary late summer-autumn peak is observed in the Balkhash-Junggar region in August–October when vegetation dies down and frequency of depressions increases (Figure 6c).

In CA, in all regions except the Aralkum, dust storms occurred in June–September but dust activity peaked in different months, starting earlier in the south, for example, in June–July in northern Afghanistan and southern Turkmenistan and in August–September elsewhere (Figure 6). Dust activity weakened significantly between November and February although a positive trend in DSA days was observed in the Karakum-Kyzylkum region in winter. In northern Afghanistan, where dust storms were more frequent in summer, they were probably more intense between October and March when a larger number of DPS was activated per day (Figure 6g).

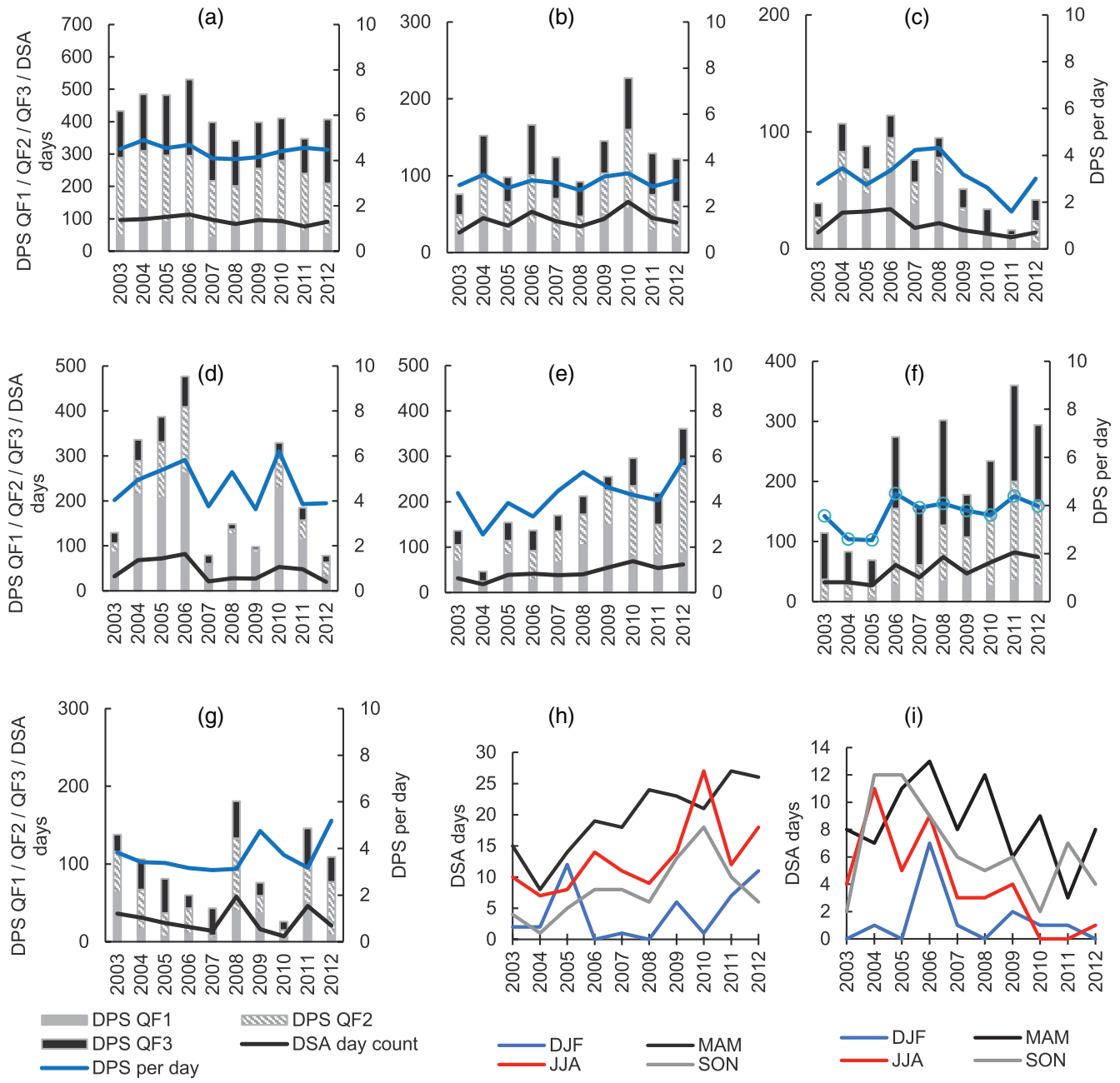

Figure 5. Interannual variability in DPS including observations awarded different quality flags (QF), number of DSA days and number of DPS activated per day: (a) Taklimakan; (b) Hexi Corridor; (c) Balkhash-Junggar; (d) Pre-Aral; (e) Aralkum; (f) Karakum-Kyzylkum; (g) Balkh Delta (upper Amu Darya). Panels (h) and (i) show seasonal totals of DSA days per year in the Aralkum and Balkhash-Junggar sub-regions, respectively. Note that scales showing DPS and DSA day counts differ between the regions. DJF statistics for 2003 (h and i) includes January and February 2003 only. Regional boundaries are shown in Figure 1. DPS, dust point sources; DSA, dust source activation.

In the Aralkum, dust sources were activated throughout the year and, while the maximum frequency was observed in April–May, it remained high in June–October and in February–March (Figure 6e). The average number of DPS per dusty day, however, was highest during the colder season from November to May (five-six DPS per day) indicating more intense dust storms. Between June and October, 3–4 DPS per day were activated. This finding is in contrast to previous studies, suggesting a summer peak in dust activities in this region (Groll et al., 2013.; Orlovsky et al., 2005; Xi & Sokolik, 2015b). In contrast to other dust source regions in CA, the dust-emitting surfaces in the Aralkum are devoid of vegetation because of the high salinity of

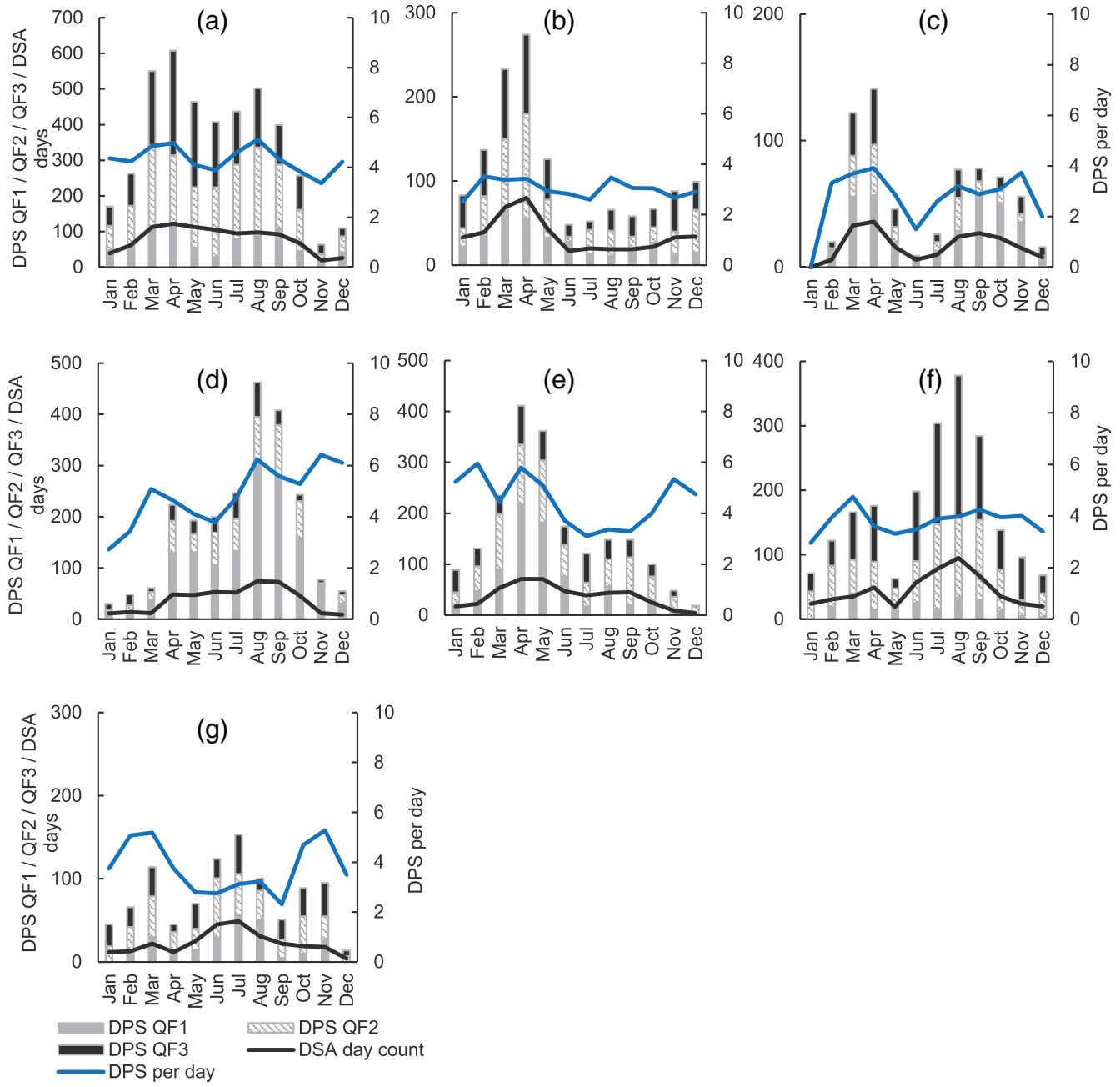

Figure 6. As in Figure 5 but for seasonal variability.

the exposed lake bed. In spring, in the absence of vegetation, lower threshold wind speeds are required to dislodge dust particles (Knippertz, 2014) while in summer, salt crusts prevent dust entrainment (Argaman et al., 2006).

4. Discussion

The deserts of CA and NWC are among the largest source regions of mineral dust in the world by area and by dust emission flux supplying up to 25% of desert aerosol to the atmosphere (Ginoux et al., 2012; Shao & Dong, 2006). Regional sources of dust are located in proximity to the major glacierized regions of High Asia and play an important role in the snow/ice-albedo feedback (Gautam et al., 2013; Painter et al., 2012),

potentially affecting snow melt in the mountains and provision of water to the arid lowlands. The development of this unique 10-years data set of DPS, which retains the 1-km resolution of satellite data, for the first time enabled a detailed assessment of dust sources in this region, using consistent observations at an appropriate spatial resolution. This data set expands dust storm and dust deposition climatologies, derived from regional historical weather station records. While these climatologies span several decades, they are sparse and many were discontinued in the 1990s in CA (Groll et al., 2013; Indoitu et al., 2012; Issanova et al., 2015b) although observations continue in the Taklimakan (Wang et al., 2006; 2008). It provides data for regions such as northern Afghanistan, where there were no previous observations. The high-resolution mapping of dust sources improves characterization of spatiotemporal variability in dust emissions derived from the AOD data by Ginoux et al. (2012) and Xi and Sokolik (2015a) by localizing dust sources within the broad dust hotspot areas defined by AOD and thus contributing to improvements in numerical dust and weather forecast models in the region (Li & Sokolik, 2017; Walker et al., 2009).

4.1. Uncertainties and Limitations of the DPS Data Set

There are several sources of uncertainty associated with this DPS data set: (i) availability of only two MODIS images per day limiting observations to a period between 10:30 and 13:30 local time; (ii) obscuration of DPS either by clouds or by pre-existing dust plumes generated upwind; (iii) limitations of the DEP algorithm; (iv) potential operator's errors of manual DPS detection.

Availability of two fixed-time acquisitions per day is a significant and recognized limitation of using MODIS data for mapping of dust sources (Miller, 2003) particularly in comparison with the application of geostationary SEVIRI data (Hennen et al., 2019; Schepanski et al., 2007). Dust mobilization is forced by meteorological processes varying in time or following diurnal cycles. In other dust source regions, for example, in the Sahara (Schepanski et al., 2007; 2009) and the Middle East (Hennen et al., 2019), dust emissions occur frequently after sunrise and breakdown of nocturnal inversions. Thus in the Middle East, dust emissions are most frequent between 6:00 and 12:00 with considerably fewer activation in the afternoon and at night. Hennen et al. (2019) assessed bias in the detection of dust emissions in the Middle East by degrading temporal resolution of SEVIRI data from 15 to 60 min showing reduction in the number of observed events particularly in summer when it is caused by the mesoscale rather than synoptic-scale processes. Using coarser temporal resolution, however, did not significantly affect the derived geographical distributions of sources, that is fewer point sources were detected in the same regions and smaller dust events were missed.

There are no data on timing of DSA in CA except the data produced by this study. However, diurnal cycles of the occurrence of dust storms, as registered by regional meteorological stations, show that their frequency peaks between 9:00 and 15:00 which is later in the day in comparison with the Middle East. Minimum is observed between 18:00 and 6:00 (Indoitu et al., 2009; 2012). We used diurnal cycles of surface wind speed, derived from ERA5 reanalysis for the study period and averaged over the subregions and meteorological seasons, as a proxy for timing of DSA (Figure S7). Across most of the study region, maximum wind speed is observed between 10:00 and 14:00 with exception of the northern and eastern sectors of the Taklimakan where wind speed peaks at 10 a.m. in summer and spring. The timing of MODIS overpasses, therefore, coincides with the diurnal maxima in wind speed (Figure S7) and dust storms occurrence (Indoitu et al., 2009; 2012) partly alleviating the problem although DSA in the afternoon may be underestimated more significantly. In the absence of geostationary data, it is impossible to assess the proportion of underestimated sources. Following Hennen et al. (2019), we suggest that statistics of DPS activation per day is underestimated but it is unlikely that spatial clustering of DPS, linked to specific landforms (Table S3), is affected to a significant extent, that is data with higher temporal resolution are expected to show more frequent DPS activations, especially with regard to smaller sources, in the same locations.

It is not possible to detect dust beneath the meteorological clouds using this dust enhancement technique (Miller, 2003) although it is more successful in discriminating between dust and clouds than other techniques (Baddock et al., 2009). The obscuration of DPS by clouds affected the northern part of the study area to a greater extent, as low-pressure systems are more frequent there, particularly in March–April and October–November. The obscuration of DPS by dust clouds affected their detection particularly in the Taklimakan, Kyzylkum, Karakum and in northern Afghanistan. Thus in the Taklimakan, where dust plumes, forming in the north and east, circulate within the closed basin for several days, the highest quality (QF1)

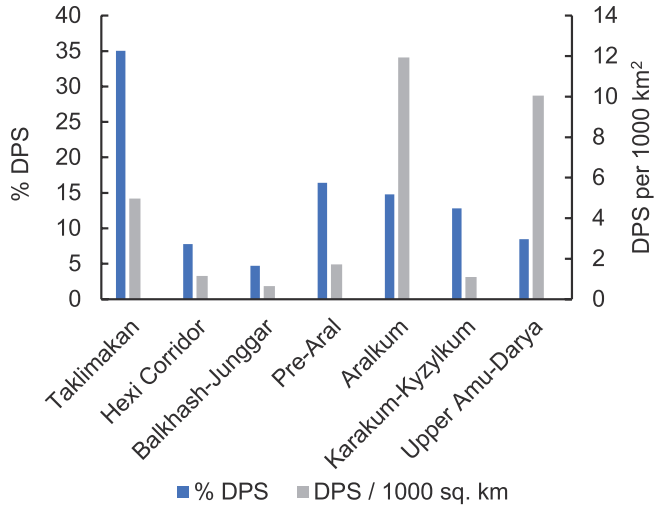

Figure 7. Percentage of DPS records in each region and average number of DPS per 1,000 km^2. Regional boundaries are shown in Figure 1. DPS, dust point sources.

DPS observations account for 7%–20% of the detected DPS between March and August and annually, between 11% (2003) and 26% (2004 and 2009) (Figures 5a and 6a). In the Karakum and Kyzylkum, less than 4% of observations accounted for QF1 DPS in 2003 and 2007 (Figure 5f). Here, higher quality observations were made in May–June (13%–22% QF1 DPS) and lower quality in July–August (5%–9% QF1 DPS) (Figure 6f). By contrast, in the north, where DPS density is lower, QF1 DPS accounted for 50%–90% of all observations (Figures 5, 6c, and 6d).

A key problem limiting the effectiveness of the DEP technique is that defining a universal threshold distinguishing between dust and nondust proved highly problematic. The DE thresholds varied between sub-regions and seasons and, in some instances, individual dust events (Figure 2). Resampling of pixel histograms to adjust the dust/nondust thresholds helped to achieve effective dust enhancement and visualization in this and other studies (Baddock et al., 2009) but made the development of the DPS data set extremely time-consuming. Varying thresholds make the development of any automated DEP algorithm problematic and compromises between quality and efficiency will be required.

4.2. Dust Point Sources versus Dust Optical Depth

Comparison of DPS locations with FO-DOD above the 0.2 threshold and with previously published AOD climatologies (Li & Sokolik, 2017; Xi & Sokolik, 2015a), showed that in many regions, there was a close match between high FO-DOD values and DPS count despite a high proportion of QF3 observations. Thus in the Karakum-Kyzylkum region, the QF1:QF2 and QF2:QF3 ratios were 0.25 and 0.83, respectively (Figures 5f and 6f) but the dust enhancement method successfully recognized DPS in the areas with the highest FO-DOD, for example, in the Syr Darya valley, over the southeastern Caspian shores and in the lower reaches of the Zeravshan (Figure 3a). DPS were successfully detected in the northern Taklimakan where QF1:QF2 and QF2:QF3 ratios were 0.58 and 0.60, respectively, and also in the eastern Taklimakan (Figure 3b), northern Afghanistan, and in those regions of the pre-Aral where atmospheric dust load was high (Figure 3a). While obscuration by dust clouds inevitably reduced accuracy of DPS mapping, these examples show that the dust enhancement technique discerns DPS in regions with high AOD. However, there was a notable lack of agreement in several regions. In the Balkhash-Junggar region (Figures 3b and S1), the discrepancy between DPS and FO-DOD can be attributed to the low density (Figure 7) and infrequent activation (Figures 5c and 6c) of sources, which did not enable build-up of dust in the atmosphere. Here, the number of DPS (dusty days) declined from 80–115 (20–32) in 2004–2008 to 16–50 (10–16) in 2009–2012 (Figure 5c). However, more often the observed discrepancy was due to the displacement of dust in the atmosphere.

A relatively low number of DPS and high FO-DOD values were identified in the central and southern Taklimakan (Figure 3b). Previous field studies showed that the sands of the central Taklimakan have low (below 4%) content of dust-sized particles and while dust sources were reported, field studies did not identify it as a major dust-producing region (Wang et al., 2006; 2008). The Dust Enhancement method successfully identified a relatively small number of aeolian DPS in the central and eastern Taklamakan (Figure 3b; Table S3) confirming these conclusions. In the southern Taklimakan, it successfully identified clusters of DPS associated with fluvial sources and alluvial piedmont fans (Figure 3b) where high frequency of dust storms was previously reported (Wang et al., 2006). However, fluvial, alluvial and lacustrine sources are less common in the south than in the north. By contrast, gravel cover and stone pavements are more widespread reducing the availability of fine material (Wang et al., 2008). We suggest that while the identified sources do generate dust locally, atmospheric dust observed over the southern Taklimakan is predominantly transported from the northern and eastern sectors of the desert and banked against the Kunlun Mountains. On 73% and 62% of all days, when dust sources were activated in the Taklimakan in spring and summer, respectively, north-easterly, north-westerly and northerly winds dominated over its southern sector indicating dust transport from the Tarim and Lop Nur regions. Modeling confirms this conclusion (Uno et al., 2005).

The Ustyurt plateau and Mangyshlak peninsula, previously identified by Xi and Sokolik (2015a) as one of the main dust hotspots in CA on the basis of high AOD and low NDVI values, were another region with high FO-DOD and very few DPS (Figures 3a and S1). The Ustyurt is predominantly a gravelly gypsiferous desert where coarse gravel, either loose or sparsely covered by *Anabasis salsa* or *Artemisia*, dominates land cover (Lioubimtseva, 2002; Viktorov, 1971). There is a notable absence of landforms associated with accumulation of dust-size material and its availability is low across the Ustyurt. Exceptions are a series of depressions containing salt pans or solonchaks on the border with the pre-Aral region and sands in the north and west of the plateau (Viktorov, 1971) where the dust enhancement method successfully identified DPS despite the high FO-DOD values (Figures 3a and S1). Modeling of dust entrainment by Li and Sokolik (2017) showed low dust emission from the Ustyurt and Mangyshlak. These results were interpreted by the authors as erroneous because they contradicted the observed high AOD but they are in agreement with the absence of DPS in this region. Analysis of the ERA5 wind fields showed that, easterly or north-easterly flow was frequent over the Aralkum throughout the year, accounting for 45% and 34% of the DSA days in spring and summer, respectively, and over the Sarygamysh region in spring, transporting dust toward the Caspian and the Ustyurt.

4.3. Comparison of the Dust Source Regions

In all, just under 13,500 DPS were detected in the study region between 2003 and 2012. The largest numbers of sources, accounting for 35% of all DPS, were registered in the Taklimakan followed by the pre-Aral region (16%) and the Aralkum (15%) (Figure 7). While the Taklimakan and the pre-Aral are vast areas occupying about 0.95×10^6 km^2 and 1.29×10^6 km^2, respectively, the Aralkum is a smaller desert characterized by the highest average density of 12 DPS per 1,000 km^2. The density of DPS in the Taklimakan was comparatively low (5 DPS per 1,000 km^2) because most DPS were concentrated along the Tarim and its tributaries and Lake Lop Nur while the central and southern Taklimakan were considerably less active (Figure 3b). An even lower density characterized the Karakum and Kyzylkum deserts where DPS were also associated with fluvial landforms and concentrated along the modern or palaeo river channels. A very high density of DPS characterized the Balkh delta (upper Amu Darya), where 8% of all DPS developed over an area which is 10 times smaller than the Taklimakan. Although meteorological aspects of DPS activation are outside the scope of this paper, we note that the threshold wind speed for dust entrainment was the lowest in the Balkh delta, with about 80% of all dust storms initiated by wind speeds of 5 m s^{-1} or less. It is also in these areas-northern and eastern Taklimakan, Aralkum, and Balkh delta-that the highest frequency of dusty days was observed (Figure 4a).

Many studies have investigated links between land surface characteristics and dust storms (e.g., Bullard et al., 2011, 2008; Xi & Sokolik, 2015b). We attempted to establish links between DPS activity and landforms using the geomorphological classification of dust-emitting surfaces developed by Bullard et al. (2011) and historical archives of high-resolution satellite imagery. A lack of detailed information about land surface properties in CA, going beyond a broad Land-Cover and Land-Use Change (LCLUC) scheme (e.g., Xi & Sokolik, 2015a; 2015b) did not allow us to conduct an in-depth analysis within the framework of this study.

In most cases, there was a clear link between land surface characteristics and development of DPS. A notable example is the formation of DPS on fire scars (Figure S4) which were the predominant sources of dust in the north, from western Kazakhstan to the Junggar basin in China (Table S3). However, attribution was more difficult in the areas without a predominant surface type, for example, at the margins of alluvial fans where cultivated farmland, fully or partially abandoned agricultural fields and natural alluvial plains exist in proximity. Under 2% of all DPS formed in such areas.

The largest number of DPS-40% of all registered in the study area-were associated with fluvial systems and alluvial deposits south of the Aral Sea and in the Taklimakan (Table S3). Dry lakes accounted for the second highest share at 29.7% of all DPS. This was typical not only of the Aralkum but also of the Taklimakan (Table S3) where DPS concentrated near the desiccated Lake Lop Nur. While dry lakes are prominent sources of dust in many regions (Bullard et al., 2011; Ginoux et al, 2012; Hennen et al., 2019; Schepanski et al., 2009; Shao et al., 2011), in CA and NWC the contemporary lake desiccation is particularly widespread (Liu et al., 2019) due to fluctuations of lake levels on a decadal timescale caused by tectonic activity (Koronkevich, 2002), excessive water abstraction for irrigation and poor water management, and the observed

climatic warming (Bai et al., 2011; Liu et al., 2019; Micklin, 2007; Middleton, 2002; Yapiyev et al., 2017). Drying lakes were identified as major sources of dust in the wider area including the Sistan basin in Afghanistan and Iran (Rashki & Kaskaoutis, 2019) and Lake Urmia basin in Iran (Ghomashi & Khalesifard, 2019). Many lakes—from Iran and Afghanistan to Kazakhstan—are saline, and the contribution of drying lakes to the formation of dust and salt storms, damaging to crops and natural ecosystems (Ge et al., 2019; Goudie et al., 2016), requires further investigation.

5. Conclusions

This study presented the first data set of dust sources in CA and NWC derived from MODIS imagery, at a spatial resolution of ~1 km which made detection of individual dust emissions possible. We compiled seasonal 1° × 1° gridded data sets of frequency of DSA days. These data helped to improve the localization of dust sources in comparison with AOD data, highlighting the eastern and northern Taklimakan, the Aralkum, northern Afghanistan and Amu Darya, Syr Darya and Uzboy valleys (but not the wider Karakum and Kyzylkum) as the most persistent sources of dust. The region between the Aral and Caspian Seas, as well as the central and southern Taklimakan, were shown to have few dust sources despite the high AOD which forms due to dust transport from the upwind sources. It is envisaged that the new data set will complement the existing meteorological station and AOD data, help to improve regional-scale dust emission and transport models and to resolve discrepancies between modeling and observations of dust in the atmosphere. We attempted a preliminary- and limited-analysis of links between dust storms and landforms in the study area. This analysis should be expanded, focusing on the role of the wildfire in the north, changing lake levels across the region, water use for irrigation and agricultural practices in the south. However, this will require detailed land surface data, which is currently limited in CA.

Data Availability Statement

Nobakht, Mohamad, Shahgedanova, Maria and White, Kevin H (2021): Coordinates of Dust Point Sources in Central Asia and Northwestern China derived from MODIS imagery, 2003–2012. University of Reading. Data set. https://researchdata.reading.ac.uk/id/eprint/281

Acknowledgments
This work was funded by the University of Reading (UK) International PhD Scholarship scheme. The authors are grateful to the anonymous reviewers for their most helpful comments. The authors declare no conflict of interest.

References

Aoki, I., Kurosaki, Y., Osada, R., Sato, T., & Kimura, F. (2005). Dust storms generated by mesoscale cold fronts in the Tarim Basin, Northwest China. *Geophysical Research Letters*, *32*(6), 1–4. https://doi.org/10.1029/2004GL021776

Argaman, E., Singer, A., & Tsoar, H. (2006). Erodibility of some crust forming soils/sediments from the Southern Aral Sea Basin as determined in a wind tunnel. *Earth Surface Processes and Landforms*, *31*(1), 47–63. https://doi.org/10.1002/esp.1230

Baddock, M. C., Bullard, J. E., & Bryant, R. G. (2009). Dust source identification using MODIS: A comparison of techniques applied to the Lake Eyre Basin, Australia. *Remote Sensing of Environment*, *113*(7), 1511–1528. https://doi.org/10.1016/j.rse.2009.03.002

Bai, J., Chen, X., Li, J., Yang, L., & Fang, H. (2011). Changes in the area of inland lakes in arid regions of central Asia during the past 30 years. *Environmental Monitoring and Assessment*, *178*(1–4), 247–256. https://doi.org/10.1007/s10661-010-1686-y

Baitulin, I. O. (2001). National strategy and action plan to combat desertification in Kazakhstan. In S.-W. Breckle, M. Veste, & W. Wucherer (Eds.), *Sustainable land use in deserts* (pp. 441–447). Berlin, Heidelberg: Springer-Verlag.

Bullard, J., Baddock, M., Mctainsh, G., & Leys, J. (2008). Sub-basin scale dust source geomorphology detected using MODIS. *Geophysical Research Letters*, *35*(March), L15404. https://doi.org/10.1029/2008GL033928

Bullard, J. E., Harrison, S. P., Baddock, M. C., Drake, N., Gill, T. E., McTainsh, G., & Sun, Y. (2011). Preferential dust sources: A geomorphological classification designed for use in global dust-cycle models. *Journal of Geophysical Research*, *116*(4), F04034. https://doi.org/10.1029/2011JF002061

Che, H., Wang, Y., Sun, J., Zhang, X., Zhang, X., & Guo, J. (2013). Variation of aerosol optical properties over the Taklimakan Desert in China. *Aerosol and Air Quality Research*, *13*(2), 777–785. https://doi.org/10.4209/aaqr.2012.07.0200

Che, H., Zhang, X.-Y., Xia, X., Goloub, P., Holben, B., Zhao, H., et al. (2015). Ground-based aerosol climatology of China: Aerosol optical depths from the China Aerosol remote sensing network (CARSNET) 2002–2013. *Atmospheric Chemistry and Physics*, *15*(13), 7619–7652. https://doi.org/10.5194/acp-15-7619-2015

Chin, M., Diehl, T., Tan, Q., Prospero, J. M., Kahn, R. A., Remer, L. A., et al. (2014). Multi-decadal aerosol variations from 1980 to 2009: A perspective from observations and a global model. *Atmospheric Chemistry and Physics*, *14*(7), 3657–3690. https://doi.org/10.5194/acp-14-3657-2014

Darmenov, A., & Sokolik, I. (2005). Identifying the regional thermal-IR radiative signature of mineral dust with MODIS. *Geophysical Research Letters*, *32*(16), L16803. https://doi.org/10.1029/2005GL023092

Gautam, R., Hsu, N. C., Lau, W. K., & Yasunari, T. J. (2013). Satellite observations of desert dust-induced Himalayan snow darkening. *40*, 988–993. https://doi.org/10.1002/GRL.50226

Ge, Y., Abuduwaili, J., & Ma, L. (2019). Lakes in arid land and saline dust storms. *E3S Web of Conferences*, *99*, 4–7. https://doi.org/10.1051/e3sconf/20199901007

Ghomashi, F., & Khalesifard, H. R. (2019). CALIPSO recordings and categorization of atmospheric aerosols over the Urmia Lake. *E3S Web of Conferences*, *99*, 3–6. https://doi.org/10.1051/e3sconf/20199901005

Gillette, D. A. (1999). A qualitative geophysical explanation for 'hot spot' dust emitting source regions. *Contributions to Atmospheric Physics*, *72*(1), 67–77.

Ginoux, P., Garbuzov, D., & Hsu, N. C. (2010). Identification of anthropogenic and natural dust sources using moderate resolution imaging spectroradiometer (MODIS) deep blue level 2 data. *Journal of Geophysical Research*, *115*(5), 1–10. https://doi.org/10.1029/2009JD012398

Ginoux, P., Prospero, J. M., Gill, T. E., Hsu, N. C., & Zhao, M. (2012). Global-scale attribution of anthropogenic and natural dust sources and their emission rates based on MODIS deep blue aerosol products. *Reviews of Geophysics*, *50*, RG3005. https://doi.org/10.1029/2012RG000388

Goudie, A., Kent, P., & Viles, H. (2016). Pan morphology, distribution and formation in Kazakhstan and neighbouring areas of the Russian federation. *Desert*, *21*(1), 1–13. https://doi.org/10.22059/jdesert.2016.58313

Goudie, A. S. (2009). Dust storms: Recent developments. *Journal of Environmental Management*, *90*(1), 89–94.

Groisman, P., Shugart, H., Kicklighter, D., Henebry, G., Tchebakova, N., Maksyutov, S., et al. (2017). Northern Eurasia future initiative (NEFI): Facing the challenges and pathways of global change in the twenty-first century. *Progress in Earth and Planetary Science*, *4*(1), 41. https://doi.org/10.1186/s40645-017-0154-5

Groll, M., Opp, C., & Aslanov, I. (2013). Spatial and temporal distribution of the dust deposition in central Asia–results from a long term monitoring program. *Aeolian Research*, *9*, 49–62. https://doi.org/10.1016/j.aeolia.2012.08.002

Hansen, A. D. A., Kapustin, V. N., Kopeikin, V. M., Gillette, D. A., & Bodhaine, B. A. (1993). Optical absorption by aerosol black carbon and dust in a desert region of Central Asia. *Atmospheric Environment Part A. General Topics*, *27*(16), 2527–2531.

Hennen, M., White, K., & Shahgedanova, M. (2019). An assessment of SEVIRI imagery at various temporal resolutions and the effect on accurate dust emission mapping. *Remote Sensing*, *11*(8), 918. https://doi.org/10.3390/rs11080965

Hofer, J., Althausen, D., Abdullaev, S. F., Makhmudov, A. N., Nazarov, B. I., Schettler, G., et al. (2017). Long-term profiling of mineral dust and pollution aerosol with multiwavelength polarization Raman Lidar at the Central Asian site of Dushanbe, Tajikistan: Case studies. *Atmospheric Chemistry and Physics*, *17*(23), 14559–14577. https://doi.org/10.5194/acp-17-14559-2017

Hofer, J., Ansmann, A., Althausen, D., Engelmann, R., Baars, H., Abdullaev, S. F., & Makhmudov, A. N. (2020). Long-term profiling of aerosol light extinction, particle mass, cloud condensation nuclei, and ice-nucleating particle concentration over Dushanbe, Tajikistan, in Central Asia. *Atmospheric Chemistry and Physics*, *20*(8), 4695–4711. https://doi.org/10.5194/acp-20-4695-2020

Holben, B. N., Tanré, D., Smirnov, A., Eck, T. F., Slutsker, I., Abuhassan, N., et al. (2001). An emerging ground-based aerosol climatology: Aerosol optical depth from AERONET. *Journal of Geophysical Research*, *106*(D11), 12067–12097. https://doi.org/10.1029/2001JD900014

Hsu, N. C., Tsay, S. C., King, M. D., & Herman, J. R. (2004). Aerosol properties over bright-reflecting source regions. *IEEE Transactions on Geoscience and Remote Sensing*, *42*(3), 557–569. https://doi.org/10.1109/TGRS.2004.824067

Indoitu, R., Kozhoridze, G., Batyrbaeva, M., Vitkovskaya, I., Orlovsky, N., Blumberg, D., & Orlovsky, L. (2015). Dust emission and environmental changes in the dried bottom of the Aral Sea. *Aeolian Research*, *17*, 101–115. https://doi.org/10.1016/j.aeolia.2015.02.004

Indoitu, R., Orlovsky, L., & Orlovsky, N. (2009). Dust storms in Middle Asia: Spatial and temporal variations. *WIT Transactions on Ecology and the Environment*, *122*, 353–364. https://doi.org/10.2495/ECO090331

Indoitu, R., Orlovsky, L., & Orlovsky, N. (2012). Dust storms in Central Asia: Spatial and temporal variations. *Journal of Arid Environments*, *85*, 62–70.

Issanova, G., Abuduwaili, J., Galayeva, O., Semenov, O., & Bazarbayeva, T. (2015). Aeolian transportation of sand and dust in the Aral Sea region. *International Journal of Environmental Science and Technology*, *12*(10), 3213–3224. https://doi.org/10.1007/s13762-015-0753-x

Issanova, G., Abuduwaili, J., Kaldybayev, A., Semenov, O., & Dedova, T. (2015). Dust storms in Kazakhstan: Frequency and division. *Journal of the Geological Society of India*, *85*(3), 348–358. https://doi.org/10.1007/s12594-015-0224-5

Issanova, G., Jilili, A., & Semenov, O. (2014). Deflation processes and their role in desertification of the southern Pre-Balkhash deserts. *Arabian Journal of Geosciences*, *7*(11), 4513–4521. https://doi.org/10.1007/s12517-013-1106-z

Jiang, L., Jiapaer, G., Bao, A., Kurban, A., Guo, H., Zheng, G., & De Maeyer, P. (2019). Monitoring the long-term desertification process and assessing the relative roles of its drivers in Central Asia. *Ecological Indicators*, *104*, 195–208. https://doi.org/10.1016/j.ecolind.2019.04.067

Knippertz, P. (2014). Meteorological aspects of dust storms. In P. Knippertz & J.-B. W. Stuut (Eds.), *Mineral dust a key player in the Earth system* (pp. 121–147). Berlin: Springer Nature.

Koronkevich, N. (2002). Rivers, lakes, inland seas and wetlands. In M. Shahgedanova (Ed.), *The physical geography of northern Eurasia* (pp. 122–148). Oxford: Oxford University Press.

Kostianoy, A. G., Lebedev, S. A., & Solovyov, D. M. (2013). Satellite monitoring of the Caspian Sea, Kara-Bogaz-Gol Bay, Sarykamysh and Altyn Asyr Lakes, and Amu Darya River. In I. S. Zonn & A. G. Kostianoy (Eds.), *The Turkmen lake Altyn Asyr and water resources in Turkmenistan. The handbook of environmental chemistry* (Vol. 28, pp. 197–231). Berlin, Heidelberg: Springer. https://doi.org/10.1007/698_2013_237

Kozhoridze, G., Orlovsky, L., & Orlovsky, N. (2012). Monitoring land cover dynamics in the Aral Sea region by remote sensing. *Earth Resources and Environmental Remote Sensing/GIS Applications III*, *8538*, 85381V. https://doi.org/10.1117/12.972306

Létolle, R., Micklin, P., Aladin, N., & Plotnikov, I. (2007). Uzboy and the Aral regressions: A hydrological approach. *Quaternary International*, *173–174*, 125–136. https://doi.org/10.1016/j.quaint.2007.03.003

Li, L., & Sokolik, I. N. (2017). Developing a dust emission procedure for Central Asia. *Air, Soil and Water Research*, *10*, 1–12. https://doi.org/10.1177/1178622117711939

Lioubimtseva, E. (2002). Arid environments. In M. Shahgedanova (Ed.), *The physical geography of northern Eurasia* (pp. 267–283). Oxford: Oxford University Press.

Liu, H., Chen, Y., Ye, Z., Li, Y., & Zhang, Q. (2019). Recent Lake Area changes in Central Asia. *Scientific Reports*, *9*(1), 1–11. https://doi.org/10.1038/s41598-019-52396-y

Mahowald, N. M. (2007). Anthropocene changes in desert area: Sensitivity to climate model predictions. *Geophysical Research Letters*, *34*(18). https://doi.org/10.1029/2007GL030472

Mahowald, N. M., Kloster, S., Engelstaedter, S., Moore, J. K., Mukhopadhyay, S., McConnell, J. R., et al. (2010). Observed 20th century desert dust variability: Impact on climate and biogeochemistry. *Atmospheric Chemistry and Physics*, *10*(22), 10875–10893. https://doi.org/10.5194/acp-10-10875-2010

Micklin, P. (2007). The Aral Sea disaster. *Annual Review of Earth and Planetary Sciences*, *35*(1), 47–72. https://doi.org/10.1146/annurev.earth.35.031306.140120

Middleton, N. (2002). The Aral Sea. In M. Shahgedanova (Ed.), *The physical geography of northern Eurasia* (pp. 497–510). Oxford: Oxford University Press.
Middleton, N. J. (1986). Dust storms in the Middle East. *Journal of Arid Environments*, *10*, 83–96.
Miller, S. D. (2003). A consolidated technique for enhancing desert dust storms with MODIS. *Geophysical Research Letters*, *30*(20), 2071. https://doi.org/10.1029/2003GL018279
Monier, E., Kicklighter, D. W., Sokolov, A. P., Zhuang, Q., Sokolik, I. N., Lawford, R., et al. (2017). A review of and perspectives on global change modeling for Northern Eurasia. *Environmental Research Letters*, *12*(8), 083001. https://doi.org/10.1088/1748-9326/aa7aae
Orlovsky, L., Matsrafi, O., Orlovsky, N., & Kouznetsov, M. (2012). Sarykamysh Lake: Collector of drainage water—the past, the present, and the future. In I. S. Zonn , A. G. Kostianoy (Eds.), The Turkmen lake Altyn Asyr and water resources in Turkmenistan. The Handbook of environmental chemistry. (Vol. 28 pp. 107–140). Berlin, Heidelberg: Springer. https://doi.org/10.1007/698_2012_191
Orlovsky, L., Orlovsky, N., & Durdyev, A. (2005). Dust storms in Turkmenistan. *Journal of Arid Environments*, *60*, 83–97. https://doi.org/10.1016/j.jaridenv.2004.02.008
Painter, T. H., Bryant, A. C., & Skiles, S. M. (2012). Radiative forcing by light absorbing impurities in snow from MODIS surface reflectance data. *Geophysical Research Letters*, *39*(17), L17502. https://doi.org/10.1029/2012GL052457
Prospero, J. M., Ginoux, P., Torres, O., Nicholson, S. E., & Gill, T. E. (2002). Environmental characterization of global sources of atmospheric soil dust identified with the Nimbus 7 Total Ozone Mapping Spectrometer (TOMS) absorbing aerosol product. *Reviews of Geophysics*, *40*(1), 2-1–2-31. https://doi.org/10.1029/2000RG000095
Qian, Y.-B., Wu, Z.-N., Yang, Q., Zhang, L.-Y., & Wang, X.-Y. (2007). Ground-surface conditions of sand-dust event occurrences in the southern Junggar Basin of Xinjiang, China. *Journal of Arid Environments*, *70*, 49–62.
Rashki, A., & Kaskaoutis, D. (2019). Assessment of the dust sources over Central and Southwest Asia with emphasis on the Sistan dust storms. *E3S Web of Conferences*, *99*, 10–13. https://doi.org/10.1051/e3sconf/20199901002
Rittner, M., Vermeesch, P., Carter, A., Bird, A., Stevens, T., Garzanti, E., et al. (2016). The provenance of Taklamakan desert sand. *Earth and Planetary Science Letters*, *437*, 127–137. https://doi.org/10.1016/j.epsl.2015.12.036
Savtchenko, A., Ouzounov, D., Ahmad, S., Acker, J., Leptoukh, G., Koziana, J., & Nickless, D. (2004). Terra and aqua MODIS products available from NASA GES DAAC. *Advances in Space Research*, *34*(4), 710–714. https://doi.org/10.1016/j.asr.2004.03.012
Sayer, A. M., Hsu, N. C., Bettenhausen, C., & Jeong, M. J. (2013). Validation and uncertainty estimates for MODIS Collection 6 'Deep Blue' aerosol data. *Journal of Geophysical Research: Atmospheres*, *118*(14), 7864–7872. https://doi.org/10.1002/jgrd.50600
Schepanski, K., Tegen, I., Laurent, B., Heinold, B., & Macke, A. (2007). A new Saharan dust source activation frequency map derived from MSG-SEVIRI IR-channels. *Geophysical Research Letters*, *34*, 1–5. https://doi.org/10.1029/2007GL030168
Schepanski, K., Tegen, I., Todd, M. C., Heinold, B., Bönisch, G., Laurent, B., & Macke, A. (2009). Meteorological processes forcing Saharan dust emission inferred from MSG-SEVIRI observations of subdaily dust source activation and numerical models. *Journal of Geophysical Research*, *114*(D10), D10201. https://doi.org/10.1029/2008JD010325
Shao, Y., & Dong, C. H. (2006). A review on East Asian dust storm climate, modelling and monitoring. *Global and Planetary Change*, *52*(1–4), 1–22. https://doi.org/10.1016/j.gloplacha.2006.02.011
Shao, Y., Wyrwoll, K., Chappell, A., Huang, J., Lin, Z., Mctainsh, G., et al. (2011). Dust cycle: An emerging core theme in Earth system science. *Aeolian Research*, *2*(4), 181–204. https://doi.org/10.1016/j.aeolia.2011.02.001
Shi, Y., Zhang, J., Reid, J. S., Hyer, E. J., & Hsu, N. C. (2013). Critical evaluation of the MODIS Deep Blue aerosol optical depth product for data assimilation over North Africa. *Atmospheric Measurement Techniques*, *6*, 949–969. https://doi.org/10.5194/amt-6-949-2013
Smirnov, V. V., Johnson, T. C., Krapivtseva, G. M., Krivchikova, T. V., & Shukurov, A. H. (1993). Synoptic meteorological conditions during the U.S.S.R./U.S. dust experiment in Tadzhikistan in September 1989. *Atmospheric Environment. Part A. General Topics*, *27*(16), 2471–2479.
Sokolik, I. N., & Golitsyn, G. (1993). Investigation of optical and radiative properties of atmospheric dust aerosols. *Atmospheric Environment Part A. General Topics*, *27*(16), 2509–2517.
SternbergT.(Ed.), (2017). *Climate hazard crises in Asian societies and environments*. Abingdon: Taylor & Francis.
Sternberg, T., & Edwards, M. (2017). Desert dust and health: A central Asian review and steppe case study. *International Journal of Environmental Research and Public Health*, *14*(11), 1–19. https://doi.org/10.3390/ijerph14111342
Strong, C. L., Bullard, J. E., Dubois, C., Mctainsh, G. H., & Baddock, M. C. (2010). Impact of wild fire on interdune ecology and sediments: An example from the Simpson Desert, Australia. *Journal of Arid Environments*, *74*(11), 1577–1581. https://doi.org/10.1016/j.jaridenv.2010.05.032
Uno, I., Harada, K., Satake, S., Hara, Y., & Wang, Z. (2005). Meteorological characteristics and dust distribution of the Tarim Basin simulated by the nesting RAMS/CFORS Dust Model. *Journal of the Meteorological Society of Japan*, *83A*(3), 219–239. https://doi.org/10.2151/jmsj.83A.219
Velichko, A., & Spasskaya, I. (2002). Climatic change and the development of landscapes. In M. Shahgedanova & A. S. Goudie (Eds.), *The physical geography of northern Eurasia* (pp. 36–69). Oxford: Oxford University Press.
Viktorov, S. V. (1971). *Pustynya Ustyurt i voprosy ee osvoeniya (The Ustyurt desert and problems of the reclamation)*. Moscow: Nauka Publishers.
Walker, A. L., Liu, M., Miller, S. D., Richardson, K. A., & Westphal, D. L. (2009). Development of a dust source database for mesoscale forecasting in southwest Asia. *Journal of Geophysical Research*, *114*(18), D18207. https://doi.org/10.1029/2008JD011541
Wang, X., Xia, D., Wang, T., Xue, X., & Li, J. (2008). Dust sources in arid and semiarid China and southern Mongolia: Impacts of geomorphological setting and surface materials. *Geomorphology*, *97*(3–4), 583–600. https://doi.org/10.1016/j.geomorph.2007.09.006
Wang, X., Zhou, Z., & Dong, Z. (2006). Control of dust emissions by geomorphic conditions, wind environments and land use in northern China: An examination based on dust storm frequency from 1960 to 2003. *Geomorphology*, *81*(3–4), 292–308. https://doi.org/10.1016/j.geomorph.2006.04.015
Washington, R., Todd, M., Middleton, N. J., & Goudie, A. S. (2003). Dust-storm source areas determined by the total Ozone monitoring Spectrometer and Surface Observations. *Annals of the Association of American Geographers*, *93*(2), 297–313. https://doi.org/10.1111/1467-8306.9302003
Xi, X., & Sokolik, I. N. (2015a). Dust interannual variability and trend in Central Asia from 2000 to 2014 and their climatic linkages. *Journal of Geophysical Research: Atmosphere*, *120*(23), 12175–12197. https://doi.org/10.1002/2015JD024092
Xi, X., & Sokolik, I. N. (2015b). Seasonal dynamics of threshold friction velocity and dust emission in Central Asia. *Journal of Geophysical Research: Atmospheres*, *120*(4), 1536–1564. https://doi.org/10.1002/2014JD022471
Xuan, J., & Sokolik, I. N. (2002). Characterization of sources and emission rates of mineral dust in Northern China. *Atmospheric Environment*, *36*(31), 4863–4876. https://doi.org/10.1016/S1352-2310(02)00585-X

Yapiyev, V., Sagintayev, Z., Inglezakis, V. J., Samarkhanov, K., & Verhoef, A. (2017). Essentials of endorheic basins and lakes: A review in the context of current and future water resource management and mitigation activities in. *Water*, *9*, 798. https://doi.org/10.3390/w9100798

Ye, Z., Chen, Y., & Zhang, X. (2014). Dynamics of runoff, river sediments and climate change in the upper reaches of the Tarim River, China. *Quaternary International*, *336*, 13–19.